Equivalent Circuits of Dipole Antennas for Broadband Applications

Binwen Wang, Hui Ning, Youjie Yan, Chengyun Cao, and Meiqi Zhu

Northwest Institute of Nuclear Technology
Xi'an, 710024, China
srxh_bingwen@aliyun.com, ninghuisun@aliyun.com, pine976@163.com, caochenhyun12@163.com,
dtzmq_126@126.com

***Abstract* –** In this paper distributed parameter equivalent circuits are developed for linear dipoles, dielectric coated dipoles and lumped loaded dipoles. Theoretical solutions for each distributed parameter and the reasonable non-uniform segmentation of antennas serve as the foundation for the derivation. The accomplished validations of the modeling procedures indicate that the given equivalent circuits are capable of correctly describing dipole antennas in frequency and time domains, with the advantages of wideband, frequency independence and unambiguous physical meaning. Relying on the presented equivalent circuits, broadband issues such as simulating input impedance, predicting equivalent lengths and computing transient responses of dipole antennas can be readily addressed. In addition, the circuit model provides helpful insights into the analysis and design for the loaded dipole antennas.

***Index Terms* –** dipole antenna, distributed parameter, equivalent circuit, non-uniform segmentation, receiving antenna, transient response.

I. INTRODUCTION

Utilizing equivalent circuits to analyze an antenna has the advantages of fast operation speed, high efficiency and less consumption of computational resources. Precise and effective equivalent circuits have emerged as powerful methods for investigating antenna radiation characteristics [1–5], coupling effects between array elements [6–7], transient response problems [8–10], loaded antennas [11–13], and antenna design and optimization [14–20]. Equivalent circuit modeling is a significant area of interest within the field of antennas. Recent studies have demonstrated that the interests of equivalent circuit modeling are wideband, frequency-independent, simple circuit topology, ease of parameter computation, clear physical meaning, and the ability to explore transient issues. For example, reference [21] sought to acquire circuit element values with least amount of effort, references [2, 22] placed emphasis on wideband, precision and clear physical meaning, and equivalent circuits in [23–24] are frequency independent realized by the proposed empirical formulas.

Usual modeling procedures can be summarized from past literature as follows: first acquire the input impedance from antenna geometry, next deal with numerical methods, intuitive approaches or comprehensive methods, then circuit topologies are suggested and the element parameters are solved, and finally verification is undertaken. Relying on extensive optimization, numerical methods can give high accuracy, but at the expense of complicated circuit topologies and absence of physical meaning. As an example, with support of a genetic algorithm, reference [25] proposed a complex equivalent circuit for dipoles, but in which a negative capacitance was introduced. The key idea of intuitive approaches is to employ reasonable RLC circuits to match the resonance phenomenon of a dipole. In this way, the circuit configurations are always simple, such as the four-element circuit in [26] and the five-element circuit in [27], however, these circuits suffered from lack of wideband precision, and the parameter solution relies on empirical formulas [23, 28] or a large number of simulations [29]. Comprehensive methods employ flexible and suitable use of both intuitive and numerical approaches. For instance, the calculation of parameter values for a plasma dipole is conducted via a genetic algorithm [30]. A wideband circuit is modeled with eigenmode methods in [2], in which the Moment Method is utilized to compute the characteristic modes.

It is worth mentioning that the five-element equivalent circuit proposed by Humaid in [27] has triggered many studies due to its concise circuit topology and clear physical meaning. For example, equivalent circuits of a dipole in a lossy medium and dielectric coated wire antenna are developed by Liao in [23, 31]. The five-element circuit model is employed to explore the radiation characteristics of the plasma dipole and monopole in [1, 30] respectively. Moreover, transient responses of dipoles excited by EMP were investigated and revealed

Submitted On: October 5, 2022
Accepted On: May 3, 2023

https://doi.org/10.13052/2023.ACES.J.380403

in [8] on the basis of the five-element circuit. However, intuitive models only work with time-harmonic occasions [2, 27], broadband or transient problems remain poorly understood, despite being of wide concern in electromagnetic vulnerability. In addition, intuitive models for analyzing lumped-loaded antennas are still unclear.

Taken together, the methods mentioned above are knowing the results in advance, namely the impedance characteristics of the antenna, then exploring the modeling approaches from the "results". By contrast, the distributed parameter equivalent circuit can be attained from antenna geometry immediately, and theoretically there is a wideband and frequency independent model [33]. To investigate the radiation characteristics of a monopole and the propagating properties of voltage and current on a dipole, the distributed parameter equivalent circuits are developed in [4] and [34], respectively, and these studies highlight the potential advantages of the distributed parameter equivalent circuit in antenna transient analysis. However, previous studies have failed to address the question of modeling procedure, critical factors and parameter solutions, e.g. equivalent circuit with uniform segmentation in [4] could not accurately describe the details of the antenna, and only one radiation resistance is involved in the circuit in [34], which is inconsistent with reality.

This study systematically reviews the modeling approaches for antenna equivalent circuits, aiming to present a wideband circuit model with simple topology and clear physical meaning. The subsequent structure of this study takes the form of four sections. Section II demonstrates the theoretical calculation of distributed parameters of a dipole. Section III establishes the equivalent circuits of radiating and receiving dipole antenna and explores how the segmentation affects the modeling accuracy. In Section IV, the validation of the present equivalent circuits is operated through experiments and numerical simulations in frequency and time domains, respectively. The final section sets out further research on the distributed parameter equivalent circuits of the dielectric coated dipole and lumped loaded dipole, with some numerical results.

II. SOLUTION FOR DISTRIBUTED PARAMETERS

It is a widely held view that the distributed parameters of dipole antenna include distributed capacitance, inductance, resistance and negligible conductance, and these values are determined by dipole geometry. In the following discussions and calculations, it is assumed that a linear dipole is placed in the cylindrical coordinate system and along the z axis, with pole length l_0 and pole radius r_0.

A. Distributed capacitance

The uniqueness theorem states that the electrical potential φ around the dipole can be solved while the pole potentials and the zero-potential boundary are given. With the support of φ which meets the Laplace equation in free space, the charge density on the pole surface can be acquired. Therefore, the distributed capacitance of the dipole is obtained in terms of definition and electromagnetic constitutive relations,

$$C(z) = -\varepsilon_0 \frac{\pi r_0}{V_0} \frac{\partial \varphi(z)}{\partial n}, \tag{1}$$

where ε_0 is the permittivity of vacuum, $\varphi(z)$ represents the potential around the dipole, and V_0 is the known pole potential. The Laplace equation in the cylindrical coordinate system is as follows, and only relating to r and z direction,

$$\nabla^2\varphi = \frac{\partial^2\varphi}{\partial r^2} + \frac{1}{r}\frac{\partial\varphi}{\partial r} + \frac{\partial^2\varphi}{\partial z^2} = 0. \tag{2}$$

Next, the central difference is utilized to replace the differential in equation (2),

$$\varphi_{i,j} = \frac{\left(\varphi_{i-1,j} + \varphi_{i+1,j} + \varphi_{i,j-1} + \varphi_{i,j+1}\right)}{4} + \frac{\left(\varphi_{i+1,j} - \varphi_{i-1,j}\right)}{8i}. \tag{3}$$

Finally, the distributed capacitance of the dipole antenna can be calculated via equation (1) and (3).

Take a dipole antenna with pole length l_0 = 0.1 m and pole radius r_0 = 0.001 m as an example. Figure 1 plots the distributed capacitance per unit length varying along pole length. It is observed that the distributed capacitance at both ends grows sharply, while the middle part remains steady. Approximately, the dipole antenna can be divided into three sectors, the sector near the feeding gap with length of $0.2l_0$, the terminal sector with length of $0.1l_0$ and the medial sector with the remaining length. This variation suggests further studies to evaluate the impact of the two former sectors on the equivalent circuit modeling.

B. Distributed inductance

The dipole antenna is considered as a short wire with total length $L_0 = 2l_0$ to derivate the distributed inductance, including external and internal inductance.

The radial current distribution within the wire is concentrated on its axis to determine the external inductance. It is assumed that the magnetic induction density at point P outside the wire is dB, which is contributed by current element Idz on the dipole antenna. Hence, the total magnetic induction density B_p can be carried out via integrating dB along the short wire,

$$B_p = \int_0^{L_0} \mathrm{d}B = \frac{\mu_0 I}{4\pi r_\mathrm{p}} \left[\frac{L_0 - z_\mathrm{p}}{\sqrt{r_\mathrm{p}^2 + \left(L_0 - z_\mathrm{p}\right)^2}} + \frac{z_\mathrm{p}}{\sqrt{r_\mathrm{p}^2 + z_\mathrm{p}^2}} \right], \tag{4}$$

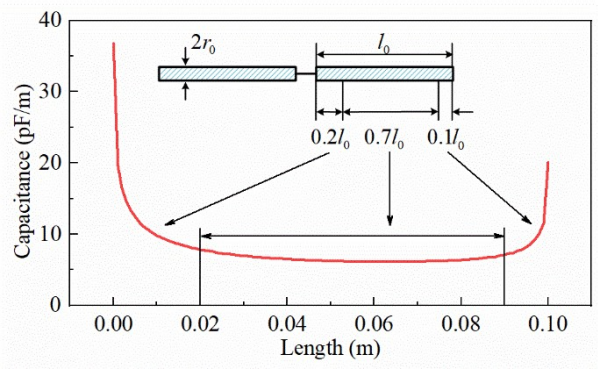

Fig. 1. Distributed capacitance per unit length of the dipole varying along the pole length.

where μ_0 is the permeability of vacuum, r_p and z_p are the position depiction of point P in the cylindrical coordinate system. Next, integrating B_p along the short wire to gain the total magnetic linkage outside the wire, then, the external inductance per unit length is derived as,

$$L_e = \frac{\mu_0}{2\pi}\left[\ln\frac{L_0+\sqrt{L_0^2+r_0^2}}{r_0} - \frac{\sqrt{L_0^2+r_0^2}}{L_0} + \frac{r_0}{L_0}\right]. \quad (5)$$

Due to the dipole antenna operating at frequencies in the order of MHz and above, the surface effect depth is almost zero, which leads to little internal inductance. Therefore, the distributed inductance of a dipole antenna is principally its external inductance.

C. Distributed resistance

Resistance consumes power in the equivalent circuit to represent the thermal loss power and the radiated power of an antenna. Compared with the latter, the former can be omitted in circuit modeling, hence, only the radiation resistance is taken into account, and this is the major contributor that the dipole is deemed to be a lossy transmission line. From the previous perspective, the concerned resistance is also distributed, and can be derived approximately based on current distribution and other distributed parameters.

Ignoring the variation of current distribution caused by radiative process, the current on the dipole is similarly sinusoidal,

$$I(z) = I_0 \sin\left[\beta\left(l_0 - |z|\right)\right], \quad (6)$$

where I_0 refers to current amplitude and β is the propagation constant.

In an attempt to derivate the distributed resistance, the dipole antenna is separated into several segments of equal length, with each radiation resistance represented by R_f. Then, the total radiant power at the operating frequency of the dipole antenna is demonstrated as follows,

$$P_f = \int_0^{l_0} \frac{1}{2} I_0^2 \sin^2\left[\beta\left(l_0 - |z|\right)\right] \mathrm{d}z R_f. \quad (7)$$

The radiant power can also be described utilizing lumped radiation resistance R_l, which is usually 73 Ω at the first resonance frequency of the dipole antenna [35]. Thus, distributed radiation resistance is denoted as,

$$R_f = \frac{2R_l}{l_0\left[1-\sin\left(2\beta l_0\right)/2\beta l_0\right]}. \quad (8)$$

Equation (8) reveals that the key to carry out the distributed resistance is the propagation constant β, which is related to the attenuation constant α,

$$\beta = \frac{2\pi}{\lambda}\sqrt{\frac{1}{2}\left[1+\sqrt{1+\frac{\alpha^2\lambda^2}{\pi^2}}\right]}, \quad (9)$$

where λ is the operating wavelength of the dipole. The lossy transmission line theory shows that α is associated with antenna distributed resistance,

$$\alpha = \frac{R_f}{2Z_c} = \frac{R_f}{2\sqrt{L_e/C}}, \quad (10)$$

where L_e and C are the distributed capacitance and inductance respectively, Z_c is the characteristic impedance along the dipole, and which can be replaced approximately by the average characteristic impedance of the parallel two-wire transmission line,

$$Z_c \approx \overline{Z_c} = 120\left(\ln\left(2l_0/r_0\right) - 1\right). \quad (11)$$

Substituting equation (11) into (10) and combining with equation (8), the attenuation constant can be derived as,

$$\alpha = \frac{R_l}{120\left(\ln\left(2l_0/r_0\right)-1\right) l_0\left[1-\sin\left(2\beta l_0\right)/2\beta l_0\right]}. \quad (12)$$

Next, by substituting equation (9) into (12) and employing the numeric iteration, the attenuation constant is obtained. Finally, the distributed radiation resistance of dipole antenna can be attained from equation (10),

$$R_f = 2\alpha \cdot \sqrt{L_e/C}. \quad (13)$$

What stands out in these deduced results is that the solution of each distributed parameter is frequency independent. In particular, the complete calculation of the distributed radiation resistance is suggested, which is a significant result, this course not having previously been described.

III. EQUIVALENT CIRCUITS

Referring to the transmission line equivalent circuit, the distributed parameter equivalent circuit for a radiating dipole antenna is derived easily, as drawn in Fig. 2, containing n segments, and the circuit elementary cell is marked by a red dotted rectangular box.

The two branches up and down of the circuit in Fig. 2 signify the two poles of the antenna, which reveals a distinct physical meaning of geometry. V is the drive voltage on the feeding point and R_k is the feeding impedance, with the value of 50 Ω typically. C_1,

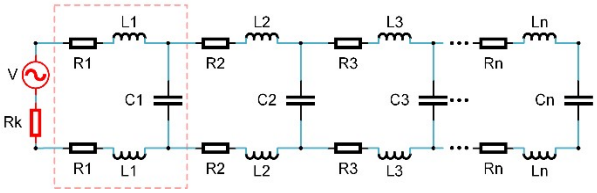

Fig. 2. Distributed parameter equivalent circuit model for radiating dipole antenna.

$C_2 \ldots C_n$ connected in parallel are the actual capacitances of each segment, determined by the corresponding segment length l_i and distributed capacitance:

$$C_i = \int_{l_i} C(l)\, dl. \tag{14}$$

The same is true of L_i and R_i in the distributed parameter equivalent circuit.

Equation (14) illustrates that the segmentation of the dipole antenna is the other decisive factor for accurate circuit modeling, which will be discussed in depth next, and then, the equivalent circuit for receiving dipole antenna are demonstrated.

A. Segmentation of dipole antenna

Obviously, the circuit topology grows more complicated as the segments increases, meanwhile cursory segmentation sacrifices the modeling accuracy. Hence, different segmentation ways are considered.

First check uniform segmentation. Four dipole antennas with different pole lengths ranging from 0.1 m to 0.3 m and with the same pole radius of 0.005 m are taken as examples, and uniform segmentations with different segment lengths are handled with these dipoles. Then, corresponding distributed parameter equivalent circuits are established to earn resonances. For easier comparison, the four dipole antennas are simulated utilizing the finite integration method. To measure the modeling accuracy, the absolute difference values between the first resonant frequencies of equivalent circuits and simulations are carried out, represented by Δf_1. Without loss of generality, the ratio of the segment length l_i to the minimum wavelength λ_{min} is employed to describe the level of uniform segmentation. The smaller the ratio, the tinier the segmentation. Figure 3 displays the curves that Δf_1 of the four dipoles vary with the ratio l_i/λ_{min}.

What stands out in Fig. 3 is that Δf_1 of different dipoles exhibit the same variation, approaching to zero as the ratio l_i/λ_{min} decreases. Peculiarly, while the ratio l_i/λ_{min} is lower than or equal to 1/10, the difference Δf_1 is less than 20 MHz, meaning that the first resonance points obtained by equivalent circuits are in good agreement with the simulated results. For most cases, the circuit of uniform segmentation with $l_i/\lambda_{min} \leq 1/10$ is adequate to accomplish time-harmonic problems for dipole antennas.

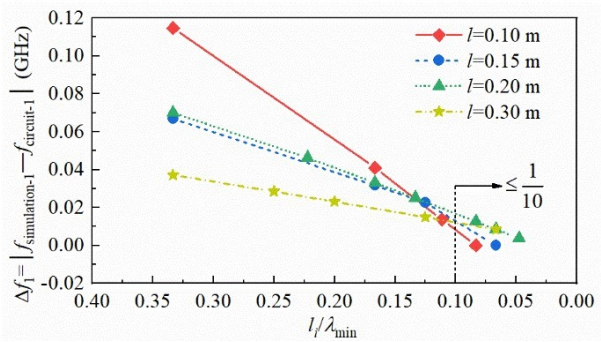

Fig. 3. Δf_1 of four dipoles varying with l_i/λ_{min}.

As inferred in Section II, distributed capacitance near the feeding gap and the terminal capacitance grows sharply, requiring fairly short segment length to handle the details mentioned. Uniform segmentation with pretty small l_i/λ_{min} can cope with this problem, but what follows is more intricate circuit topology containing massive RLC cells. Consequently, non-uniform segmentation is indispensable.

Take the antenna with pole length l_0 = 0.1 m in Fig. 3 as an instance, on the basis of uniform segmentation with l_i/λ_{min} less than 1/10, the sector near the feeding gap and the end sector are segmented again. Then, the circuit of non-uniform segmentation and the return loss are derived, and compared with other results in Fig. 4.

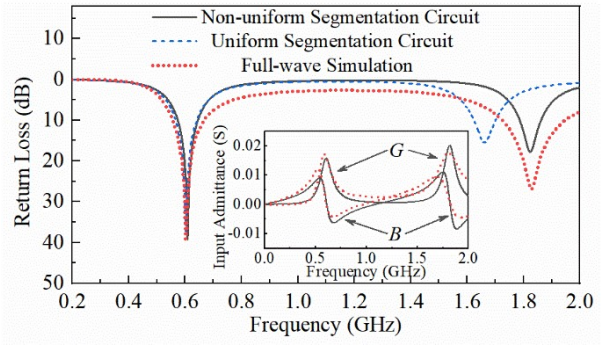

Fig. 4. Comparisons of return loss and input admittance obtained by simulation and equivalent circuits.

As can be seen from Fig. 4, consistency of the three methods at the first resonance point of the dipole antenna is achieved, which is a reasonable result and implies that further segmentation brings few effects to the first resonance. However, there is a significant difference at the second resonance, that is the circuit of non-uniform segmentation agrees well with the simulation, but differs from the circuit of uniform segmentation.

This phenomenon illustrates that simple uniform segmentation with the ratio l_i/λ_{min} less than 1/10 leads to

an equivalent circuit lack of wideband accuracy, and further segmentation to the sectors with distributed capacitance varying rapidly is of great significance in broadband equivalent circuit modeling. Meanwhile, the comparison of input admittance in Fig. 4 further proves that the equivalent circuit with the presented segmentation method exhibits wideband characteristics. Therefore, in order to handle the transient and broadband problems for a dipole antenna, the non-uniform segmentation is essential, and due to the middle sector of a dipole remaining unchanged in further segmentation, the complexity of circuit topology is reduced. However, previous reports make no attempt to consider the important role played by segmentation.

B. Equivalent circuit for receiving dipole

The principle of reciprocity in antenna theory states that the receiving mode characteristics are identical to those of transmitting mode. Thus, the distributed parameter equivalent circuit can also be employed to simulate the receiving antenna, with consideration of the induced electro motives generated by the incoming plane wave. As shown in Fig. 5, to construct the receiving equivalent circuit, the induced electro motives V_{ei} are added to the elementary cell marked in Fig. 2, with the element values unchanged.

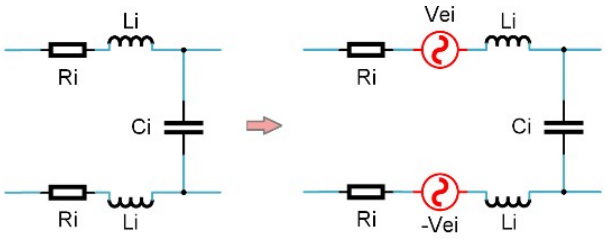

Fig. 5. Transformation of the elementary cell of equivalent circuit.

In general circumstances, the segment lengths are small enough, and each segment of the antenna can then be regarded as short dipole, leading to corresponding induced electro motives expressed approximately as follows:

$$V_{ei}(t) \approx E_i(t) l_i \cos\varphi, \tag{15}$$

where E_i is the incident electromagnetic pulse, φ is the polarization angle, and l_i is the segment length. It is believed that the two branches up and down of the receiving circuit form a current loop, with the equal values and opposite signs of the induced electro motives of each segment.

IV. VALIDATION

To validate the presented equivalent circuit, two linear dipole antennas are measured and simulated in this section. The two antennas are dipole A with pole length $l_a = 0.127$ m and pole radius $r_a = 0.0017$ m and dipole B with pole length $l_b = 0.156$ m and radius $r_b = 0.0013$ m. With the help of the theoretical solutions in the previous sections, the component values of the equivalent circuit for the two dipoles are displayed in Table 1, and the numerical simulations are operated via finite integration techniques.

Table 1: Component values of the equivalent circuits for Dipole A and B

No.	Dipole A			Dipole B		
	C/pF	*L*/nH	*R*/Ω	*C*/pF	*L*/nH	*R*/Ω
1	0.058	2.81	0.97	0.110	8.17	2.64
2	0.040	3.28	1.47	0.056	7.66	3.30
3	0.033	3.28	1.62	0.093	15.33	7.23
4	0.026	2.81	1.46	0.084	15.33	7.66
5	0.050	6.09	3.33	0.079	15.33	7.90
6	0.046	6.09	3.48	0.15	30.65	16.15
7	0.085	12.19	7.29	0.074	15.33	8.13
8	0.073	11.25	6.92	0.075	15.33	8.08
9	0.073	11.72	7.35	0.078	15.33	7.91
10	0.072	11.72	7.42	0.098	15.33	7.09
11	0.072	11.72	7.44	—		
12	0.073	11.72	7.40	—		
13	0.079	12.19	7.53	—		
14	0.043	6.09	3.61	—		
15	0.055	6.09	3.20	—		

A. Reflection coefficient

Reflection coefficients of dipole A and dipole B in frequency range of 1 MHz to 2 GHz are swept utilizing a VNA in microwave anechoic chamber. Then, the measurements are compared with the results carried out by equivalent circuits and simulations in Fig. 6. It is quite clear that, for the two dipoles, the results of equivalent circuits are consistent with the measurements and simulations.

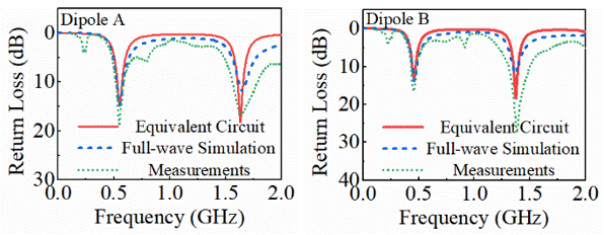

Fig. 6. Comparison of reflection coefficients for the two dipole antennas.

B. Effective length

The effective length of the antenna is usually employed to determine the induced voltage on the open-circuit terminals and also it is related to the far-zone field radiated by the antenna [35]. Both the equivalent circuit and numerical simulation can easily reveal effective lengths of the two dipoles. Measurements are handled based on the two-antenna method, and the measurements scene is shown in Fig. 7.

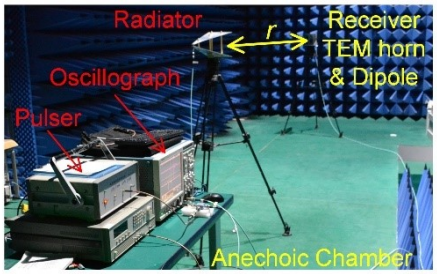

Fig. 7. Measurements scene of effective length.

Firstly, two identical TEM horns are adopted as radiating and receiving antennas respectively, and then the effective length of the TEM horn antenna can be derived via the two-antenna method as follows,

$$h_e(\omega) = \sqrt{\frac{2\pi r Z_t S_{21-t}(\omega)}{-j\omega\mu}} e^{-jkr}, \tag{16}$$

where r is the distance between radiating and receiving TEM horns, Z_t = 50 Ω is terminal load of the receiving horn, $S_{21-t}(\omega)$ is the transmission coefficient between the two horns which is measured by vector network analyzer, μ is the permeability of vacuum.

Keeping the measurement configuration unchanged, replace the receiving horn by dipole A and B in sequence. Then, the corresponding transmission coefficients are measured. On combining the measured results with $h_e(\omega)$, we deduce the effective lengths of the dipoles,

$$h_d(\omega) = S_{21-d}(\omega) \frac{2\pi r Z_t}{-j\omega\mu e^{-jkr}} \frac{1}{h_e(\omega)}. \tag{17}$$

Comparisons of the effective lengths for dipole A and B are depicted in Fig. 8. It is indicated that the effective lengths derived by equivalent circuits are mainly consistent with the simulated and measured results, only a few discrepancies are observed between the measurements and the other two methods, which may be caused by measurement inaccuracies.

C. Transient response

To examine the suitability of handling with broadband problems via equivalent circuit, transient responses of the two dipoles are demonstrated in this section. The experiment configuration is the same as Fig. 7.

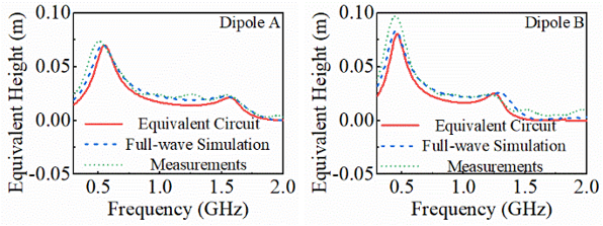

Fig. 8. Comparisons of the derived effective lengths for dipole A and B.

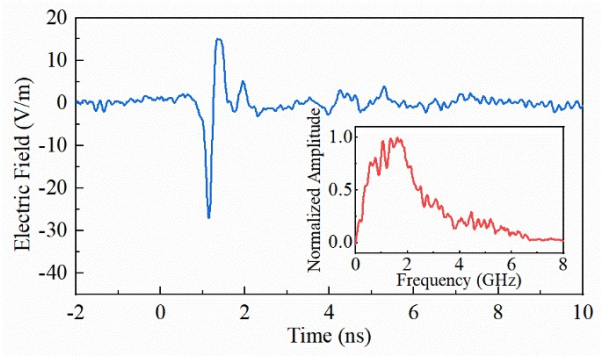

Fig. 9. Incident E-field wave and the normalized spectrum.

Figure 9 shows the measured incident E-field, generated by an ultra-wideband pulser and a radiator. Transient responses are attained with polarization matching and the arrival direction aiming at the maximum reception direction of dipoles, and compared with simulated and circuital transient responses, as depicted in Fig. 10.

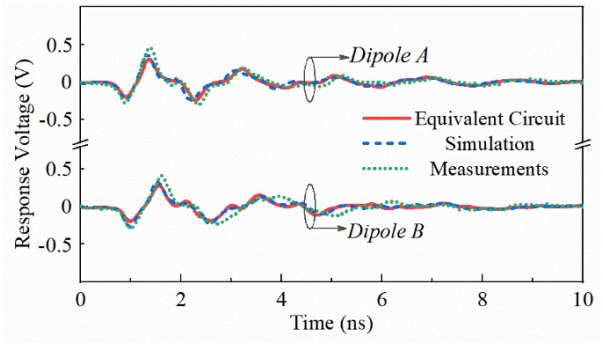

Fig. 10. Transient voltage responses of the two dipoles.

From the graph above, we can see that, for each dipole, good coherence of the transient response variations obtained by three methods are observed, both the pulse of duration and oscillating feature positions on waves.

These validations highlight that the solutions of distributed parameters directly from antenna geometry and

the modeling procedure are proper on the whole. Also, it proves that the presented equivalent circuit exhibits wideband accuracy, which is capable of being utilized to predict effective length and to investigate transient problems for dipoles.

V. APPLICATION

In this section, the distributed parameter equivalent circuits for a dielectric coated dipole and a lumped loaded dipole are derived and discussed as an application of the presented circuit model.

A. Circuit for dielectric coated dipole

Dielectric coating can protect antennas from corrosion, and is also widely applied to antenna miniaturization. For dipole antennas, dielectric coating just brings mutations to the distributed parameters, with the circuit topology unchanged, for radiating and receiving roles.

First derive the distributed parameters. A dielectric coating dipole can be transformed into a dipole with a purely magnetic coating, as demonstrated in [36], using a quasi-static approximation method. A purely magnetic coating causes little impact on capacitance of the dipole, so that a dielectric coated dipole can be further transformed into a dipole without any coating to solve its distributed capacitances. Figure 11 draws the cross sections of the three mentioned dipoles and the equivalence relationships among them. Notably, the materials considered here are homogenous, isotropic and low-loss.

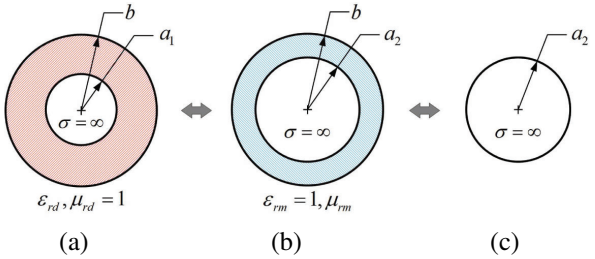

Fig. 11. Cross sections of dipoles. (a) dipole with coating dielectric, (b) dipole with coating magnetic material, and (c) dipole without any coating.

As shown in Fig. 11, the dipole with a coating of magnetic material is the equivalent one to the dipole in Fig. 11 (a), with the outer radius of coating b unchanged, and the inner radius a_1 is changed to a_2,

$$a_2 = b\left(a_1/b\right)^{1/\varepsilon_{rd}}, \tag{18}$$

ε_{rd} becomes $\varepsilon_{rm}=1$, and μ_{rd} becomes μ_{rm},

$$\mu_{rm} = \varepsilon_{rd}\mu_{rd}. \tag{19}$$

Taking away the magnetic coating, the dipole in Fig. 11 (b) is transformed to the third dipole antenna, without changing the radius a_2. Next, relying on the presented method in Section II.A, the distributed capacitance of the dielectric coating dipole can be obtained by calculating the distributed capacitance of the dipole without any coating in Fig. 11 (c).

The distributed inductance of the dielectric coated dipole comprises the inductance of the dipole in Fig. 11 (c) and the additional inductance per unit length brought by the magnetic coating in Fig. 11 (b). The former represented by L_m can be calculated via equation (5), and the latter has been induced in [37],

$$L_a = \frac{\mu_0}{2\pi}\left[\mu_{rm} - 1\right]\ln\left(\frac{b}{a_2}\right). \tag{20}$$

In general, distributed resistance engenders little effect to antenna resonances, so that the solution of distributed resistance for a dielectric coated dipole is the same as the dipole without any coating.

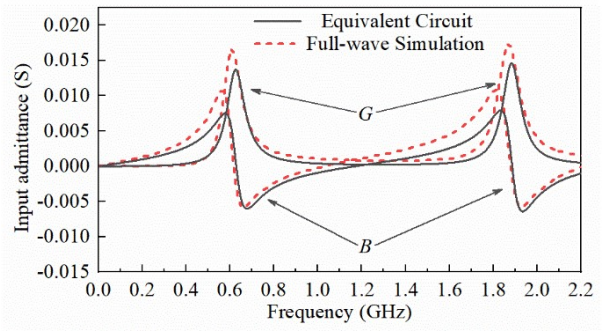

Fig. 12. Input conductance (G) and susceptance (B) of the dielectric coated dipole.

The considered sample geometry is a center-driven wire antenna with pole length of 0.1 m and pole radius of 0.001 m, covered with dielectric material of relative permittivity ε_{cd} = 3 and outer radius is 0.002 m. Finite integration techniques are employed to simulate the input admittances of the antenna and then compared with the results gained by the distributed parameter equivalent circuit, as drawn in Fig. 12, in which reasonable agreements are observed for the two methods.

To investigate the transient response of a receiving role, a Gaussian pulse with the rise time of 0.3 ns and amplitude of 1 kV/m is utilized as the incident E-field. Figure 13 compares the output voltage responses attained by full wave simulation and its equivalent circuit, agreements are achieved, and only the amplitudes are slightly discrepant.

B. Circuit for lumped loaded dipole

Loading lumped elements can significantly improve radiation performances [38–41]. In most situations, lumped loading position is not reflected by a lumped parameter equivalent circuit precisely, but it can be achieved by a distributed parameter equivalent circuit, relying on clear geometric physical meaning. Thus, it is

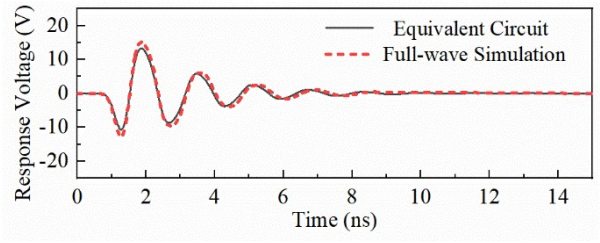

Fig. 13. Time domain responses of the dielectric coated dipole excited by Gaussian pulse.

foreseeable that the distributed parameter equivalent circuit is a convenient and efficient way to investigate the lumped loaded dipole antenna.

In this section, a dipole loaded with a parallel RLC resonant circuit is demonstrated. The RLC resonant circuit is located at the symmetrical positions of the antenna poles, as shown in Fig. 14, in which the loaded component values are R_0 = 1 kΩ, L_0 = 20 nH, C_0 = 5.5 pF.

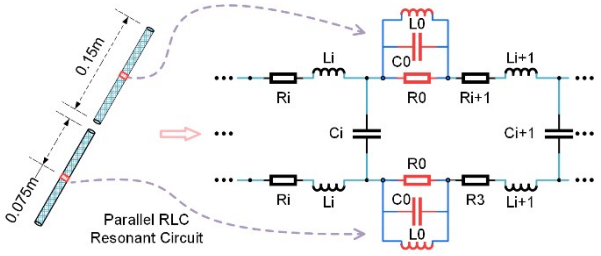

Fig. 14. A dipole loaded with parallel RLC circuit.

The input admittances of the antenna gained by simulation and the equivalent circuit are plotted and compared in Fig. 15, where the agreements and three resonances are observed, two of them are the intrinsic resonant points of the dipole antenna, and the other one is the resonance caused by the loaded RLC resonant circuit.

Using the same Gaussian pulse in Section V.A as the incident E-field, the output voltage responses and the voltages in loaded resistance are carried out by numerical simulation and equivalent circuit, and compared in Fig. 16. It is indicated that the transient voltage responses obtained by the two methods are grossly consistent, so are the voltages on R_0, while the amplitudes are slightly different.

This section demonstrates two applications of the distributed parameter equivalent circuit, for simulating a dielectric coated dipole and a lumped loaded dipole respectively. Final results indicate that the equivalent circuits can accurately describe the performances in frequency and time domain of the two antennas. In particular, the presented equivalent circuit provides useful insights into the design of a lumped loaded dipole, e.g. the loading component values and loading position can be optimized by parameter sweeping utilizing circuit simulation software quickly and efficiently, with less computational time and resources.

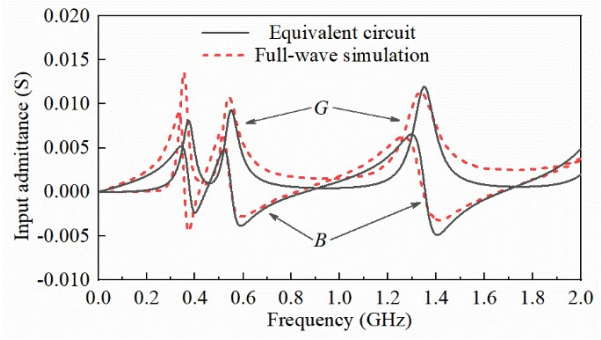

Fig. 15. Input conductance (G) and susceptance (B) of the lumped loaded dipole antenna.

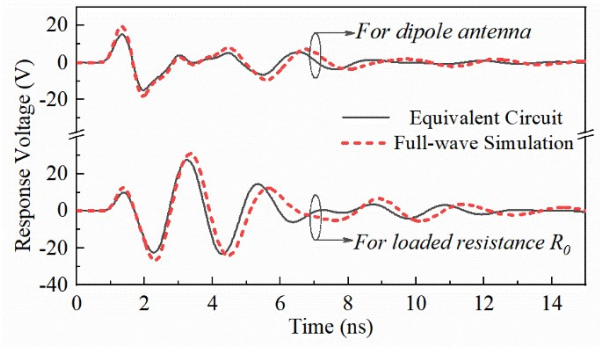

Fig. 16. Time domain responses of lumped loaded dipole excited by Gaussian pulse.

VI. CONCLUSION

The aim of this paper is to contribute to the systematic and complete understanding and modeling of distributed parameter equivalent circuits for dipoles. All distributed parameters have been theoretically derived as the modeling foundation, and reasonable non-uniform segmentation is employed to increase available bandwidth and reduce the complexity of circuit topology. The validations operated in frequency and time domains proves that the presented equivalent circuits and modeling approaches are accurate and have the advantages of broadband, frequency independence and clear physical meaning, which meets modeling expectations. Utilizing this equivalent circuit, broadband problems such as simulating input impedance and investigating transient responses can be carried out. Finally, we extend the distributed parameter equivalent circuit to dielectric

coated dipoles and lumped loaded dipoles, which provides useful insights into the analysis and design for the two dipoles.

Future work focuses on modeling distributed parameter equivalent circuits for wideband antennas, as well as predicting the near-field radiation characteristics distribution of radiating antenna and investigating the out-of-band coupling characteristics of receiving antenna based on distributed parameter equivalent circuits.

REFERENCES

[1] F. Sadeghikia, "Analysis of plasma monopole antenna using numerical method and an equivalent circuit," *IEEE Antennas Wireless Propagt. Lett.*, vol. 16, pp. 1711-1714, 2017.

[2] J. J. Adams and J. T. Bernhard, "Broadband equivalent circuit models for antenna impedances and fields using characteristic modes," *IEEE Trans. Antennas Propagat.*, vol. 61, no. 8, pp. 3985-3994, Aug. 2013.

[3] M. H. Ucar, A. Sondas, and Y. E. Erdemli, "Dual-band loop-loaded printed dipole antenna with a wideband microstrip balun structure," *Applied Computational Electromagnetics Society (ACES) Journal*, vol. 27, no. 6, pp. 458-465, June 2012.

[4] J. Bemardes, F. Peterkin, B. Hankla, and J. Latess, "Antenna circuit model for time-domain transient analysis," *IEEE 12th International Pulsed Power Conference*, Monterey, CA, pp. 260-263, June 1999.

[5] M. H. Ucar and Y. E. Erdemli, "Triple-band microstripline-fed printed wide-slot antenna for WiMAX/WLAN operations," *Applied Computational Electromagnetics Society (ACES) Journal*, vol. 29, no. 10, pp. 793-800, Oct. 2014.

[6] Y. Tak, J. Park, and S. Nam, "Equivalent circuit of a two-element spherical small antenna," in *IEEE International Symposium on Antennas and Propagation*, North Charleston, SC, pp. 1-4, June 2009.

[7] B. Riviere, H. Jeuland, and S. Bolioli, "New equivalent circuit model for a broadband optimization of dipole arrays," *IEEE Antennas Wireless Propagt. Lett.*, vol. 13, pp. 1300-1304, June 2014.

[8] Y. Liao, X. J. Ying, G. C. Shi, and Y. Wang, "Time domain response analysis with equivalent circuit models for dipole antennas under EMP," *IEEE 6th International Symposium on Antennas and Propagation and EMC Technology*, Shanghai, pp. 379-382, Oct. 2015.

[9] Y. Xiao, F. Zhu, S Zhuang, and Y. Yang, "Research on EMI of traction network transient current pulse on shielded cable terminal load," *Applied Computational Electromagnetics Society (ACES) Journal*, vol. 37, no. 4, pp. 485-496, Apr. 2022.

[10] B. Li, J. J. Wang, X. W. Song, and D. L. Su, "Equivalent circuit model of frequency-domain responses with external field," *IEEE International Symposium on Electromagnetic Compatibility*, Dresden, pp. 761-766, Aug. 2015.

[11] B. R. Strickland and N. F. Audeh, "Diode-loaded dipole antenna modeling and design," *IEEE Trans. Antennas Propagat.*, vol. 41, no. 3, pp. 333-337, Mar. 1993.

[12] B. R. Strickland and N. F. Audeh, "Numerical analysis technique for diode-loaded dipole antennas," *IEEE Trans. Electromagn. Compat.*, vol. 35, no. 4, pp. 480-483, Nov. 1993.

[13] S. Palud, F. Colombel, M. Himdi, and C. L. Meins, "Circuit modeling of a small broadband conical antenna," *IEEE Antennas Wireless Propagt. Lett.*, vol. 8, pp. 96-99, Jan. 2009.

[14] R. Li, T. Wu, B. Pan, K. Lim, J. Laskar, and M. M. Tentzeris, "Equivalent-circuit analysis of a broadband printed dipole with adjusted integrated balun and an array for base station applications," *IEEE Trans. Antennas Propagat.*, vol. 57, no. 7, pp. 2180-2184, July 2009.

[15] M. Ojaroudi and E. Mehrshahi, "Bandwidth enhancement of small square monopole antennas by using defected structures based on time domain reflectometry analysis for UWB applications," *Applied Computational Electromagnetics Society (ACES) Journal*, vol. 28, no. 7, pp. 620-627, July 2013.

[16] H. C. Jing, X. J. Xu, and Y. E. Wang. "Direct antenna modulation (DAM) with switched patch antenna performance analysis," *Applied Computational Electromagnetics Society (ACES) Journal*, vol. 29, no. 5, pp. 368-382, May 2014.

[17] J. Zolghadr, Y. Cai, and N. Ojaroudi, "UWB slot antenna with band-notched property with time domain modeling based on genetic algorithm optimization," *Applied Computational Electromagnetics Society (ACES) Journal*, vol. 31, no. 8, pp. 926-932, Aug. 2016.

[18] K. H. Yeap and W. Ismail, "Analytical model for E-shaped microstrip patch antenna," *Applied Computational Electromagnetics Society (ACES) Journal*, vol. 32, no. 4, pp. 332-338, Apr. 2017.

[19] P. Nayeri, A. Elsherbeni, R. Hasse, and D. Kajfez, "Half-loop segmented antenna with omnidirectional hemispherical coverage for wireless communications," *Applied Computational Electromagnetics Society (ACES) Journal*, vol. 33, no. 2, pp. 123-126, Feb. 2018.

[20] N. R. Kumar, P. D. Sathya, S. K. A. Rahim, and A. A. Eteng, "Reduced cross-polarization patch

antenna with optimized impedance matching using a complimentary split ring resonator and slots as defected ground structure," *Applied Computational Electromagnetics Society (ACES) Journal*, vol. 36, no. 6, pp. 718-725, June 2021.

[21] T. L. Simpson, "A wideband equivalent circuit electric dipoles," *IEEE Trans. Antennas Propagat*., vol. 68, no. 11, pp. 7636-7639, Nov. 2020.

[22] T. L. Simpson, "Equivalent circuits for electric dipoles," *IEEE International Symposium on Antennas and Propagation and North American Radio Science*, Montreal, QC, pp. 443-444, July 2020.

[23] Y. Liao, T. H. Hubing, and D. L. Su. "Equivalent circuit for dipole antennas in a lossy medium," *IEEE Trans. Antennas Propagat*., vol. 60, no. 8, pp. 3950-3953, Aug. 2012.

[24] O. O. Olaode, W. D. Palmer, and W. T. Joines, "Characterization of meander dipole antennas with a geometry-based, frequency-independent lumped element model," *IEEE Antennas Wireless Propagt. Lett*., vol. 11, pp. 346-349, 2012.

[25] B. Long, P. Werner, and D. Werner, "A simple broadband dipole equivalent circuit model," *IEEE International Symposium on Antennas and Propagation and National Radio Science*, Salt Lake City, UT, pp. 1046-1049, July 2000.

[26] T. G. Tang, Q. M. Tieng, and M. W. Gunn, "Equivalent circuit of a dipole antenna using frequency-independent lumped elements," *IEEE Trans. Antennas Propagat*., vol. 41, no. 1, pp. 100-103, Aug. 1993.

[27] M. Hamid and R. Hamid, "Equivalent circuit of dipole antenna of arbitrary length," *IEEE Trans. Antennas Propagat*., vol. 45, no. 11, pp. 1695-1696, Nov. 1997.

[28] B. H. Li and Q. Zhu, "Equivalent circuits of dipole and periodic metal rod array," *IEEE MTT-S International Microwave Symposium*, Baltimore, MD, pp. 1-4, June 2011.

[29] K. Rambabu, M. Ramesh, and A. T. Kalghatgi, "Broadband equivalent circuit of a dipole antenna," *IEE Proc.-Microw. Antennas Propagt*., vol. 146, no. 6, pp. 391-393, Dec. 1999.

[30] M. M. Badawy, H. A. E. Malhat, S. H. Zainud-Deen, and K. H. Awadalla, "A simple equivalent circuit model for plasma dipole antenna," *IEEE Trans. Plasma Sci*., vol. 43, no. 12, pp. 4092-4098, Dec. 2015.

[31] Y. Liao, T. H. Hubing, and D. L. Su, "Equivalent circuit with frequency-independent lumped elements for coated wire antennas," *IEEE Trans. Antennas Propagat*., vol. 60, no. 11, pp. 5419-5423, Nov. 2012.

[32] B. W. Wang, H. Ning, Y. J. Yan, Z. Liu, F. H. Huang, and C. Y. Cao, "Analyzing out-of band response characteristics of dipole antenna by equivalent circuit," *Modern Applied Physics*, vol. 9, no. 1, pp. 75-81, Mar. 2018.

[33] H. Zhang, J. H. Wang, and W. Y. Liang, "Study on the applicability of extracted distributed circuit parameters of non-uniform transmission lines by equivalent circuit method," *Journal of Electromagnetic Waves and Applications*, vol. 22, no. 5, pp. 839-848, 2008.

[34] J. H. Wang, "Analysis of the propagating properties of pulse voltage and current on dipole antennas by equivalent circuit method," *Acta Physica. Sinica*., vol. 49, no. 9, pp. 1693-1701, Sept. 2000.

[35] C. A. Balanis, *Antenna Theory: Analysis and Design*, John Wiley & Sons, Hoboken, NJ, USA, 2005.

[36] B. D. Popović and A. Nešić, "Generalisation of the concept of equivalent radius of thin cylindrical antennas," *IEE Proceedings*, vol. 131, no. 3, pp. 153-158, June 1984.

[37] J. Moore and M. A. West, "Simplified analysis of coated wire antennas and scatterers," *IEE Proc.-Microw. Antennas Propag*., vol. 142, no. 1, pp. 14-18, Feb. 1995.

[38] W. Samuel and A. V. Pham, "The ultrawideband elliptical resistively loaded vee dipole," *IEEE Trans. Antennas Propagat*., vol. 68, no. 4, pp. 2523-2530, Apr. 2019.

[39] Y. Xia, Y. Li, and W. Xue, "A low profile miniaturization low frequency wideband antenna using passive lumped elements loading," *Applied Computational Electromagnetics Society (ACES) Journal*, vol. 35, no. 1, pp. 31-37, Jan. 2018.

[40] W. Kang, K. W. Kim, and W. Kim, "A broad-band conductively-loaded slot antenna for pulse radiation," *IEEE Trans. Antennas Propagat*., vol. 62, no. 1, pp. 33-39, Jan. 2013.

[41] W. Kang, K. W. Kim, and I. Kim, "Implementation and analysis of discretely loaded resistive dipoles using planar resistor technology," *IEEE Trans. Antennas Propagat*., vol. 63, no. 11, pp. 5088-5093, Nov. 2015.

Binwen Wang was born in Gansu, China, in 1993. He received his B.S. degree in Nuclear Science from Xi'an Jiaotong University, Xi'an, China, in 2015, and his M.S. degree in Electro-magnetic Field and Microwave Technology from the Northwest Institute of Nuclear Technology, Xi'an, China, in 2017. He is currently an Engineer at the Northwest Institute of Nuclear Technology. His research interests include time-domain electromagnetics and ultra-wideband antenna.

Hui Ning was born in Zhejiang, China, in 1969. He received his M.S. and Ph.D. degrees in Nuclear Science and Technology from Tsinghua University, Beijing, China, in 1997 and 2001, respectively. He is currently a Professor at the Northwest Institute of Nuclear Technology, Xi'an China, specializing in time-domain electromagnetics and the pulsed power technique and its applications.

Youjie Yan was born in Henan, China, in 1982. He received his B.S. degree in Electronical Information Science and Technology from Xidian University, Xi'an China, in 2005, his M.S. degree in Electromagnetic Field and Microwave Technology from the Northwest Institute of Nuclear Technology, Xi'an, China, in 2008, and his Ph.D. degree in Plasma Physics from the University of Electronic Science and Technology of China, Chengdu, China. He is currently a Professor-level senior engineer. His research interests include time-domain electromagnetics and electromagnetic compatibility.

Chengyun Cao was born in Qinghai, China, in 1994. He received his B.S. and M.S. degrees in Electromagnetic Field and Microwave Technology from the National Defense University of Science and Technology, Changsha, China, in 2016. He is currently an Engineer at the Northwest Institute of Nuclear Technology, specializing in ultra-wideband antenna.

Meiqi Zhu was born in Jiangsu, China, in 1998. She received her B.S. degree in Electromagnetic Field and Microwave Technology from the National Defense University of Science and Technology, Changsha, China, in 2019. She is currently an Assistant Engineer at the Northwest Institute of Nuclear Technology, specializing in high power pulsers.